Published in final edited form as:
Opt Lett. 2008 May 15; 33(10): 1135–1137.

Combined Raman spectroscopy and optical coherence tomography device for tissue characterization

Chetan A. Patil[1,*], **Nienke Bosschaart**[2,3], **Matthew D. Keller**[1], **Ton G. van Leeuwen**[2,3], and **Anita Mahadevan-Jansen**[1]

[1]Department of Biomedical Engineering, Vanderbilt University, Station B Box 351631, Nashville, Tennessee 37235, USA [2]Biophysical Engineering Group, Faculty of Science and Technology, University of Twente, P.O. Box 217, 7500AE Enschede, The Netherlands [3]Laser Center, Academic Medical Center, University of Amsterdam, P.O. Box 22660, 1100 DD Amsterdam, The Netherlands

Abstract

We report a dual-modal device capable of sequential acquisition of Raman spectroscopy (RS) and optical coherence tomography (OCT) along a common optical axis. The device enhances application of both RS and OCT by precisely guiding RS acquisition with OCT images while also compensating for the lack of molecular specificity in OCT with the biochemical specificity of RS. We characterize the system performance and demonstrate the capability to identify structurally ambiguous features within an OCT image with RS in a scattering phantom, guide acquisition of RS from a localized malignancy in *ex vivo* breast tissue, and perform *in vivo* tissue analysis of a scab.

Optical imaging and spectroscopy have both been used to detect disease based on the analysis of tissue microstructure and biochemical composition, yet neither method has demonstrated the spatial sensitivity and rapid data acquisition needed for screening in combination with the high specificity required for reliable multiclass discrimination. Spectroscopy excels at detecting molecular markers of disease with high specificity, while imaging excels in detecting tissue microstructure with high sensitivity. In particular, near-infrared (NIR) Raman spectroscopy (RS) has been used for *in vivo* detection of cancers in various organs [1]. RS is sensitive to vibrational modes in tissue and produces fingerprint spectra characteristic of specific molecules and their environments, thus realizing unparalleled molecular specificity. A recent comparison of Raman, fluorescence, and diffuse reflectance spectroscopy for breast cancer detection demonstrated the superior specificity of RS in classifying disease [2]. The weak nature of RS requires integration times of 3–30 s, limiting the technique to point measurements and motivating the need for image guidance to improve sampling accuracy. A combined confocal microscopy–confocal RS device was developed to guide RS acquisition with images of tissue microstructure [3], but confocal imaging depth in epithelial tissues is limited to 250 ≈μm and the transverse field-of-view (FOV) is limited to ≈500 μm. Combining the molecular specificity of RS with an imaging method that has increased depth and larger FOV will yield a valuable tool for the early detection of disease.

Optical coherence tomography (OCT) can image over larger transverse areas of tissue (>5 mm) with micrometer scale resolution, real-time speed, and sensitivity to microstructural features

*Corresponding author: E-mail: c.patil@vanderbilt.edu.

OCIS codes: 170.4500, 170.5660, 170.6510.

of disease [4]. The primary limitation of OCT is that the images are reflectivity maps of sample morphology but lack biochemical specificity. Just as RS would benefit from image guidance, OCT would benefit from biochemical specificity for classifying irregular structures. A number of intrinsic and extrinsic approaches to add molecular contrast directly to OCT are being evaluated by many groups [5]. One of these is an OCT system capable of detecting coherent anti-Stokes RS (CARS) [6]; however, CARS requires a much costlier laser source than NIR RS and currently has limited clinical translatability. Another approach is to combine a molecularly specific method directly with OCT, such as an OCT-fluorescence device [7]. However, the higher specificity of RS makes it a better choice for detecting disease. The complementary natures of RS and OCT were demonstrated in a study where two separate instruments were used to analyze the microstructural and biochemical features of dental caries [8]. This work suggests the benefit of a single device capable of RS and OCT for complete tissue characterization.

In this Letter, we present a dual-modal RS-OCT device capable of sequentially acquiring NIR RS and OCT data through common sampling optics, while keeping the source and detection arms separate. This system allows each technique to compensate for the limitations of the other; OCT imaging can be performed in real time and can be used to guide the measurement of a Raman spectrum from an area of 600 μm in depth by 75 μm across along the central axis of the OCT image. Raman spectra can be acquired to specifically characterize the biochemical fingerprint of ambiguous structures within an OCT image. Conversely, OCT can rapidly perform micro-structural imaging of large areas and precisely guide Optical Society of America the acquisition of RS from tissue. The capabilities of RS-OCT are demonstrated in scattering phantoms, *ex vivo* tissue, and *in vivo* skin.

The instrument setup is shown in Fig. 1. A 1310 nm ($\Delta\lambda_{FWHM}$=60 nm) OCT source is coupled into a fiber Michelson interferometer with a circulator in the source arm to enable balanced detection [9]. A 50/50 fiber coupler splits the light into the reference arm [10], and the sample arm, where an *XY* galvanometer pair scans the light across an achromatic doublet objective lens (*f*=35.0 mm, NA=0.36) to generate *B* scans. The detected interference signal is band pass filtered, amplified in hardware, and digitized at 1.25M samples/s. Demodulation and logarithmic compression are performed in software prior to live display of the grayscale image.

The Raman source is a 785 nm diode laser that is directed through a magnifying lens pair that spatially filters and shapes the beam to produce a Gaussian profile. The OCT and Raman incident beams are coaligned by a dichroic mirror (DM1) and then redirected to the sample by a second dichroic mirror (DM2) that reflects both source beams while transmitting the Raman Stokes band. The *XY* galvanometers are fixed, and RS is performed only along the central axis of the objective lens. The Raman laser power at the sample is fixed at 40 mW. For Raman detection, a long-pass filter reduces Rayleigh scatter, and an achromat (*f*=19.0 mm, NA=0.33) couples the Raman scatter into a 100 μm core fiber that acts as a pinhole. An *f*/1.8 holographic imaging spectrograph with an integrated 785 nm notch filter disperses the light onto a back-illuminated, deep depletion thermoelectrically cooled CCD camera. The spectral resolution of the system is 7.7 cm^{-1}. System calibration and processing are performed using a quartz tungsten halogen lamp, a neon–argon lamp, and Raman standards (described in [11]).

All OCT images were acquired with a line rate of 500 Hz and scan range of 2.4 mm at 1 frame/s. The OCT signal to noise (SNR) is 125 dB with a mirror as the sample. The measured axial and lateral resolutions are 21 μm in air (15 μm in tissue) by 25 μm, respectively. The average Raman SNR of an RS standard such as naphthalene was found to be 57 dB with 1 s integration. The RS point-spread function (PSF) was found to be 600 μm axially and 75 μm laterally at FWHM. This was obtained axially by measuring the 1308 cm^{-1} peak intensity of a 12.5 μm layer of polyethylene as a function of its axial position in the OCT image and transversely by

measuring the falloff in Raman intensity while translating across a clean edge of the polyethylene placed at the focus of the axial PSF. To verify the coalignment of the Raman and OCT beams, a gelatin phantom was placed at multiple depths in the OCT image, and a dehydrated indentation in the surface of the sample was created with the Raman laser at high power. An OC T image of the indentation verified the transverse position of the Raman beam. A vertical targeting line at this position was overlaid onto the OCT image to guide positioning of the area of interest for RS, and horizontal targeting lines corresponding to the FWHM of the axial PSF were overlaid for axial alignment (see Fig. 2). All samples were placed on a translation stage and Raman spectra were obtained by positioning the area of interest in the sample within the three targeting lines. Figure 2–Figure 4 each display an overview OCT image of the sample; the vertical lines in these figures identify the transverse position where Raman spectra were acquired. The horizontal lines that guide the depth of RS acquisition.are the shown

A scattering gelatin phantom containing two Raman active crystals [naphthalene and 1,4-Bis (2-methylstyryl)-benzene (BMSB)] with similar optical and structural properties was used to demonstrate the ability of RS to aid OCT (Fig. 2). Although the two crystals appear similar in OCT, RS of the left crystal contains the BSMB peaks at 1181, 1206, 1594, and 1629 cm^{-1}, while the right crystal shows naphthalene peaks at 513, 765, 1024, 1381, and 1577 cm^{-1}.

The ability of OCT to screen tissues and guide RS was demonstrated with an *ex vivo* malignant human breast tissue sample (Fig. 3). The tissue was scanned with OCT to locate highly scattering abnormal regions, one of which was surrounded by normal fatty tissue. The OCT display was used to guide collection of Raman spectra from both the abnormal and normal sites. The spectral line shapes are characteristic of reported normal and malignant breast tissues [2], with the normal spectrum dominated by lipid signatures and the malignant spectrum demonstrating greater DNA and protein content, especially collagen. The size of the malignant region in Fig. 3 was only ≈500 μm, yet OCT allowed sample localization and confirmed that spectra were acquired from the correct transverse position.

The applicability of RS-OCT for *in vivo* tissue characterization was demonstrated by evaluating a healing wound on the finger of a volunteer (Fig. 4). The scab is visible in OCT as a hyperreflective region in the center of the image. Immediately adjacent to the scab is a region with epidermal disruption that is likely due to remodeling. The finger was positioned with OCT such that RS could be acquired from the center of the scab and the peripheral wound. Three spectra from each position were averaged, yielding an *in vivo* SNR of 33 dB at the 1440 cm^{-1} peak. Subtle differences in the spectral line shapes were observed, including the 856 and 940 cm^{-1} collagen peaks in the scab spectrum.

To the best of our knowledge, this Letter presents the first combined NIR RS-OCT device that demonstrates the potential advantages of morphological and biochemical evaluation of tissues. Our goal is to improve optical diagnosis of epithelial cancers with RS-OCT; however, thorough tissue characterization with RS-OCT can benefit other applications. The Raman collection throughput can be improved with filter and dichroic mirror redesign, reducing *in vivo* integration times to <10 s. The axial resolution of RS could be improved to approach that of OCT with true confocal detection, but the sharp focus of the incident beam in such a system would degrade OCT transverse resolution away from the focal plane. Using a common wavelength for RS and OCT would further simplify the RS-OCT system, but attempting RS at wavelengths closer to 1310 would result in weaker scattering and thus longer integration times. Alternatively, OCT can be performed in the 800 nm band, but increased scattering would reduce imaging depth. This system presents a compromise for optimal performance by both modalities.

Acknowledgments

The authors acknowledge contributions from E. Duco Jansen of Vanderbilt University and the Biomedical Technology Institute of the University of Twente.

References

1. Mahadevan-Jansen, A. Biomedical Photonics Handbook. Vo Dinh, T., editor. CRC Press; 2003. p. 30
2. Majumder SK, Keller MD, Kelley MC, Boulos FI, Mahadevan-Jansen A. Comparison of autofluorescence, diffuse reflectance, and Raman spectroscopy for breast tissue discrimination. J. Biomed. Opt. (to be published).
3. Caspers PJ, Lucassen GW, Puppels GJ. Biophys. J 2003;85:572. [PubMed: 12829511]
4. Fujimoto JG, Brezinski ME, Tearney GJ, Boppart SA, Bouma B, Hee MR, Southern JF, Swanson EA. Nat. Med 1995;1:970. [PubMed: 7585229]
5. Yang CH. Photochem. Photobiol. Sci 2005;81:215.
6. Vinegoni C, Bredfeldt JS, Marks DL, Boppart SA. Opt. Express 2004;12:331. [PubMed: 19471542]
7. Tumlinson AR, Hariri LP, Utzinger U, Barton JK. Appl. Opt 2004;43:113. [PubMed: 14714651]
8. Ko AC, Choo-Smith LP, Hewko M, Leonardi L, Sowa MG, Dong CC, Williams P, Cleghorn B. J.Biomed. Opt 2005;10:031118. [PubMed: 16229643]
9. Rollins AM, Izatt JA. Opt. Lett 1999;24:1484. [PubMed: 18079840]
10. Rollins AM, Kulkarni MD, Yazdanfar S, Ungarunyawee R, Izatt JA. Opt. Express 1998;3:219. [PubMed: 19384364]
11. Robichaux-Viehoever A, Kanter EM, Shappell H, Billheimer D, Jones H III, Mahadevan-Jansen A. Appl. Spectrosc 2007;61:986. [PubMed: 17910796]

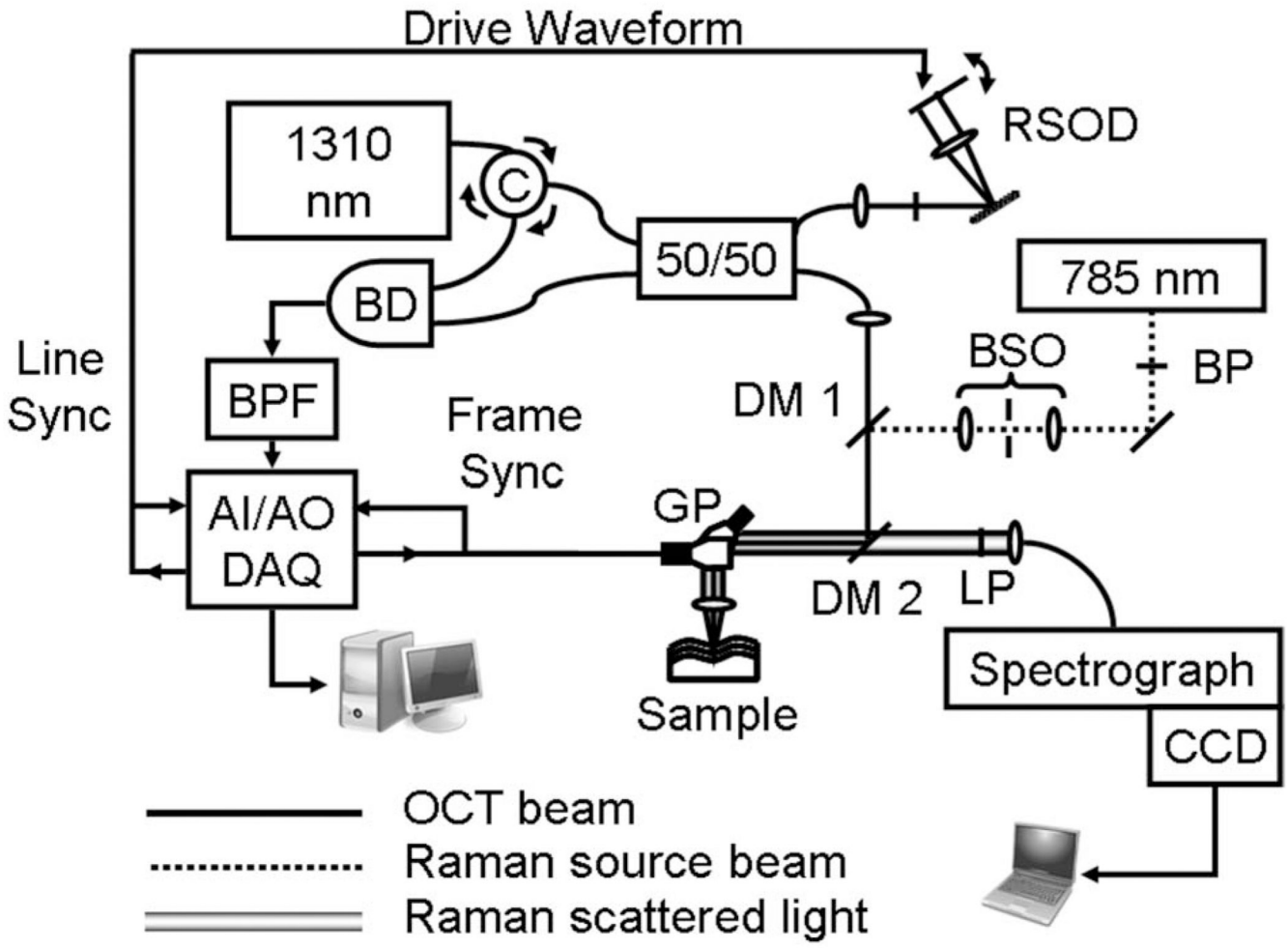

Fig. 1.

Diagram of RS-OCT system. C, circulator; RSOD, rapid scanning optical delay; BP, 785 bandpass; BSO, beam shaping optics; DM1, dichroic mirror at 990 nm; DM2, dichroic mirror at 800–950 nm; LP, long pass at 808 nm; GP, galvanometer pair; BD, balanced detector; BPF, electronic bandpass filter; AI–AO DAQ, analog input–output data acquisition.

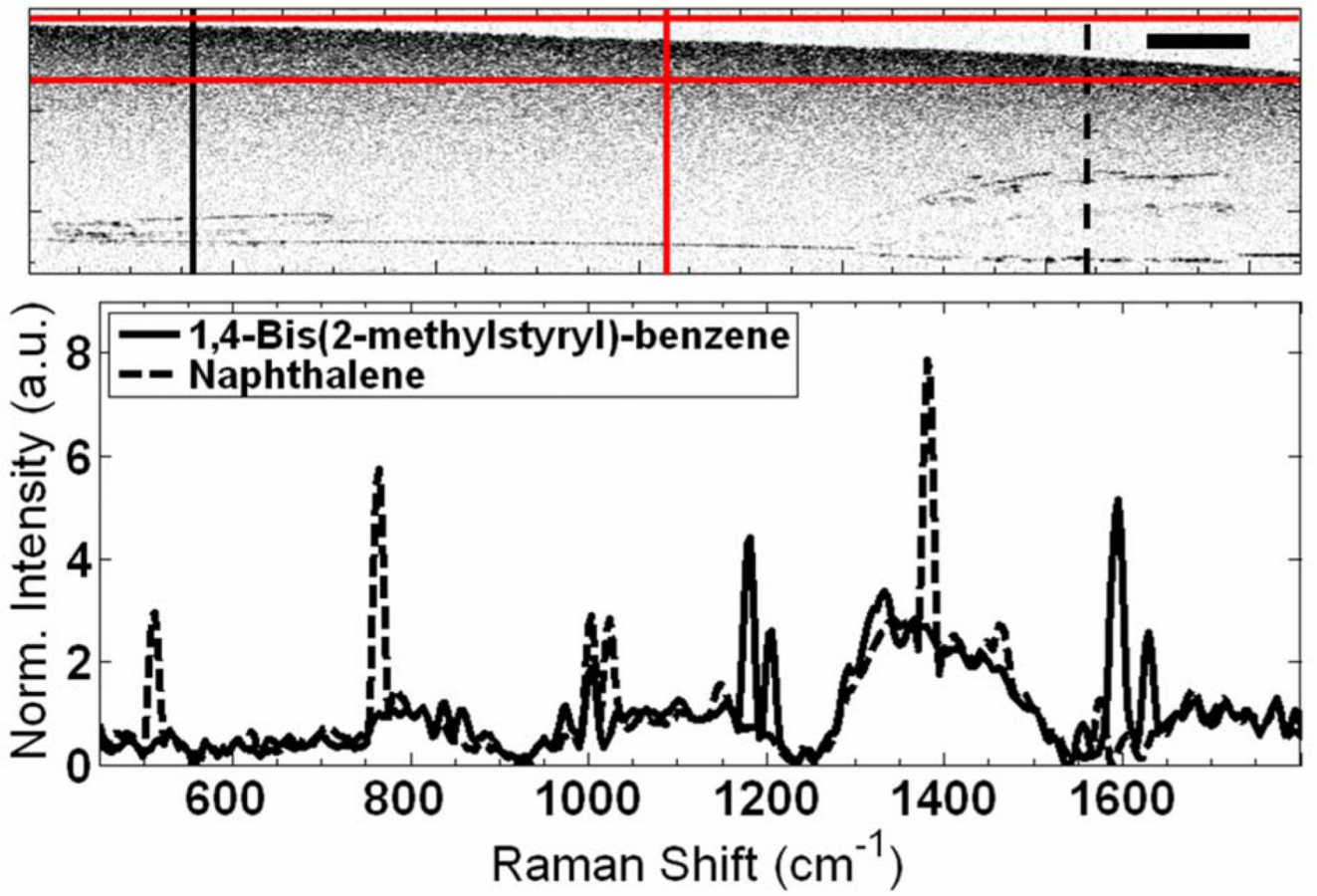

Fig. 2.

(Color online) RS-OCT from a scattering gel with BMSB (solid curve) and naphthalene (dashed curve) showing similarities in OCT but biochemical differences in RS. Scale bar is 0.8 mm. An example of the red Raman targeting lines are shown. Scattering in the sample is due to 1 μm polystyrene microspheres, whose spectral contribution can be seen from the common peak at 1001 cm^{-1}.

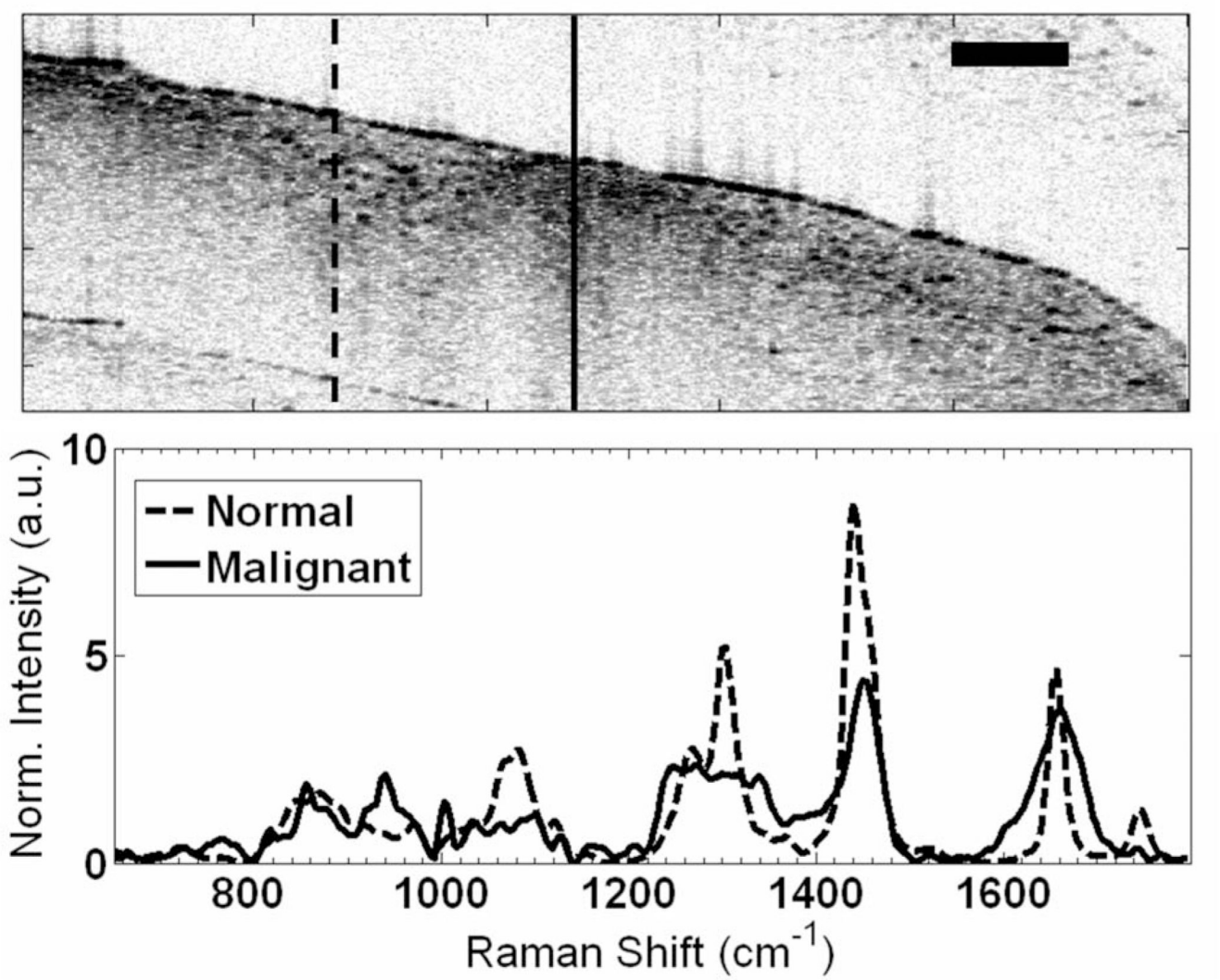

Fig. 3.
RS-OCT of normal (dashed curve) and malignant (solid curve) *ex vivo* breast sample where structural anomaly in OCT is spectrally characterized by pronounced protein peaks indicative of malignancy, while normal breast shows a strong lipid signature. Scale bar is 500μm.

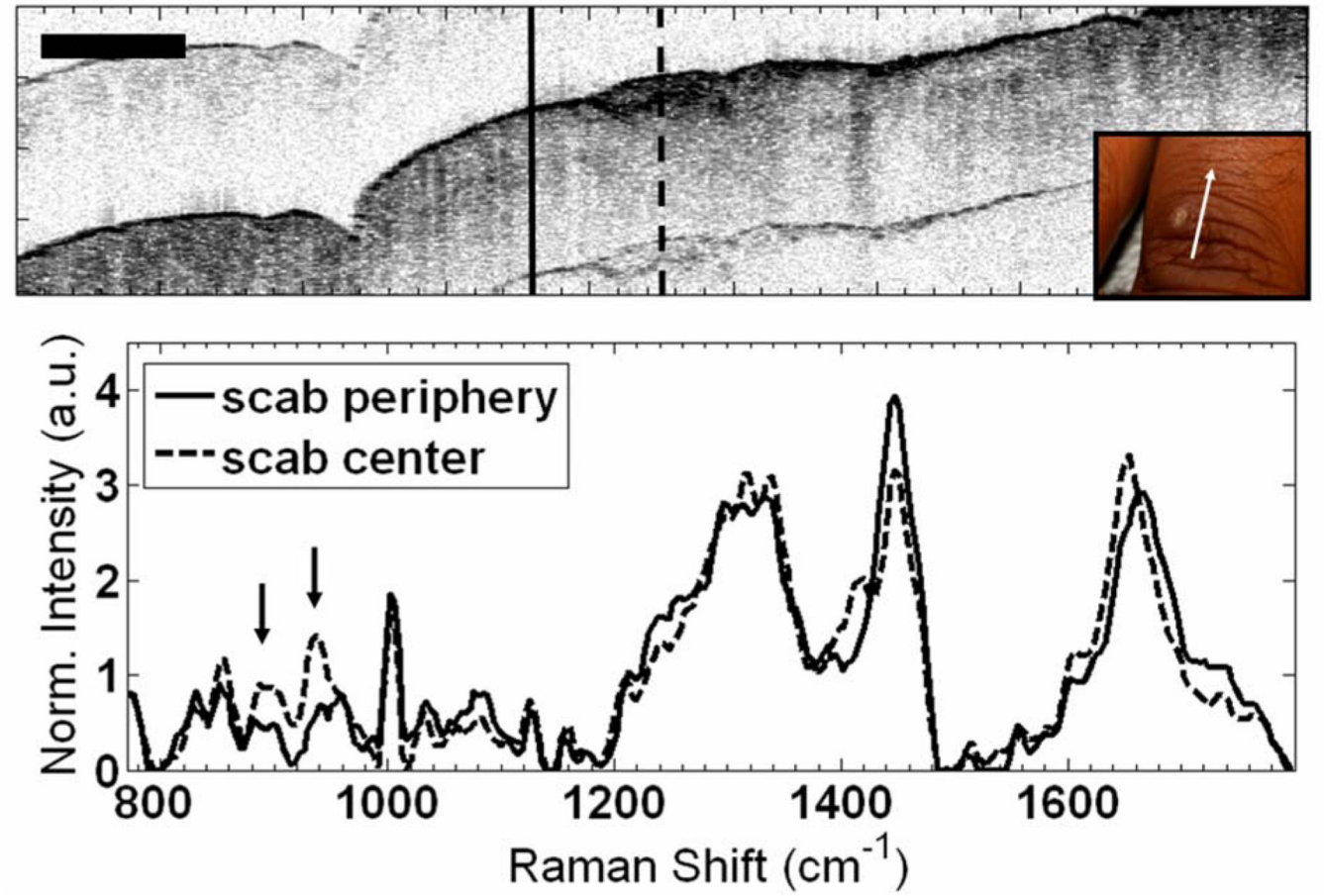

Fig. 4.

(Color online) *In vivo* RS-OCT of a scab (dashed curve) and peripheral wound (solid curve) on the back of the finger. Scale bar is 1 mm. Inset shows wound and direction of scan. Arrows identify increased collagen peaks in scab spectrum.